Efficient continuous-wave Tm,Ho:CaF2 laser at 2.1 μm

Kirill Eremeev, Pavel Loiko, Abdelmjid Benayad, Gurvan Brasse, Patrice Camy, Alain Braud

Efficient continuous-wave Tm,Ho:CaF_2 laser at 2.1 µm

KIRILL EREMEEV, PAVEL LOIKO, ABDELMJID BENAYAD, GURVAN BRASSE, PATRICE CAMY AND ALAIN BRAUD*

Centre de Recherche sur les Ions, les Matériaux et la Photonique (CIMAP), UMR 6252 CEA-CNRS-ENSICAEN, Université de Caen Normandie, 6 Boulevard du Maréchal Juin, 14050 Caen Cedex 4, France
**Corresponding author: alain.braud@ensicaen.fr*

Received XX Month XXXX; revised XX Month, XXXX; accepted XX Month XXXX; posted XX Month XXXX (Doc. ID XXXXX); published XX Month XXXX

We report on the first continuous-wave laser operation of a Tm^{3+},Ho^{3+}-codoped calcium fluoride crystal at ~2.1 µm. Tm,Ho:CaF_2 crystals were grown by the Bridgman method and their spectroscopic properties were studied. The stimulated-emission cross-section for the $^5I_7 \rightarrow {}^5I_8$ Ho^{3+} transition is 0.72×10^{-20} cm^2 at 2042 nm and the thermal equilibrium decay time is 11.0 ms. A 3 at.% Tm, 0.3 at.% Ho:CaF_2 laser generated 737 mW at 2062-2088 nm with a slope efficiency of 28.0% and a laser threshold of 133 mW. A continuous wavelength tuning between 1985 - 2114 nm (tuning range: 129 nm) was demonstrated. The Tm,Ho:CaF_2 crystals are promising for ultrashort pulse generation at ~2 µm. 2023 Optical Society of America

http://dx.doi.org/10.1364/OL.99.099999

Calcium fluoride (CaF_2) is a cubic crystal (sp. gr. *Fm*3*m*). Ca^{2+} cations are bonded in a body-centered cubic geometry to eight F^- anions. Due to its broadband transparency (0.13 – 10 µm), low refractive index (n = 1.424 at ~2 µm) and high thermal conductivity (κ = 9.7 $Wm^{-1}K^{-1}$), CaF_2 is widely used in optical components. It is also very attractive for doping with laser-active trivalent rare-earth ions (RE^{3+}) replacing for the Ca^{2+} cations [1-3]. Even at moderate doping levels (>0.1 at.% RE^{3+}), calcium fluoride crystals exhibit RE^{3+} ion clustering [4,5] resulting in a strong inhomogeneous broadening of absorption and emission bands (a "glassy-like" behavior) and enhancement of the energy-transfer processes [6]. The broadband emission and good thermal properties of RE^{3+}-doped CaF_2 crystals determine their applications in high-power / high-energy ultrafast lasers and amplifiers at ~1 µm (for Yb^{3+} and Nd^{3+} doping) [7,8], as well as broadly tunable lasers at ~2 µm (Tm^{3+} doping) [9,10].

Holmium ions (Ho^{3+}) ions (electronic configuration: [Xe]$4f^{10}$) are known for their emission in the eye-safe spectral range at ~2 µm originating from the $^5I_7 \rightarrow {}^5I_8$ transition [11]. Ho lasers emitting slightly above 2 µm are of interest for LIght Detection And Ranging (LIDAR) systems for gas sensing and wind mapping, medical applications, material processing and pumping of mid-infrared laser sources, such as Cr^{2+} lasers and optical parametric oscillators based on non-oxide crystals.

There exist two approaches for excitation of Ho^{3+} ions to the $^5I_7$ metastable state: (i) Tm^{3+},Ho^{3+} codoping [11,12] and (ii) resonant (in-band) pumping [13,14]. In the first approach, the Tm^{3+} ions (donors, D) efficiently absorb the pump radiation at ~0.8 µm (the spectral range well addressed by commercial and high power AlGaAs laser diodes) and non-radiatively transfer their energy to Ho^{3+} ones (acceptors, A), $^3F_4(Tm^{3+}) \rightarrow {}^5I_7(Ho^{3+})$. The predominantly unidirectional energy transfer (ET) D → A is maintained by an appropriate Ho^{3+}/Tm^{3+} codoping ratio, between 1:5 to 1:10, while the reduced energy-transfer upconversion (ETU) from the $^5I_7$ Ho^{3+} metastable state is ensured by choosing relatively low Ho^{3+} doping levels (<0.5 at.%). Efficient Tm,Ho lasers exist [12,15]. The codoping is also beneficial for combining the gain bandwidths of both ions, which is attractive for broadly tunable and mode-locked lasers at ~2 µm [16]. The thermal issues of Tm,Ho lasers can be mitigated by applying the fiber laser geometry [17].

Resonant pumping of Ho^{3+} ions directly to the upper laser level presents a costly alternative to the codoping scheme because of the need of expensive and complex pump sources, such as Tm fiber lasers [14] or GaSb-based laser diodes [15]. In-band pumping offers higher laser slope efficiencies [18] and weaker heat loading as compared to the codoping scheme.

The multi-site behavior of low-doped Ho:CaF_2 crystals was studied [19]. In 1965, the first lasing on the $^5S_2 \rightarrow {}^5I_8$ transition in Ho:CaF_2 was reported at 77 K [20]. Recently, the interest shifted to in-band pumped Ho:CaF_2 lasers operating on the $^5I_7 \rightarrow {}^5I_8$ transition [21-23]. Jelínek *et al.* reported on a cryogenic (83 K) continuous-wave (CW) 0.5 at.% Ho:CaF_2 laser pumped by a Tm fiber laser at 1940 nm delivering an output power of 2.37 W at 2060 nm with a slope efficiency η of 23% [21]. Duan *et al.* reported on a continuous-wave room-temperature 1 at.% Ho:CaF_2 laser with a similar pump source generating 6.94 W at 2101 nm with a higher η of 57.9% [23]. Šulc *et al.* reported on a free-running 2 at.% Tm, 0.3 at.% Ho:CaF_2 *ceramic* laser diode-pumped at 785 nm delivering an output pulse energy of 4.1 mJ at 2099 nm with η = 10.8% being tunable from 2016 to 2111 nm [24]. The same group employed a 1700 nm laser diode for Tm resonant pumping and a peak output power of 30 mW at 2074 nm was extracted with still low η of 5.3% [25].

In the present work, we report on the growth, spectroscopy and room-temperature continuous-wave laser operation of Tm^{3+}, Ho^{3+}-

codoped CaF_2 crystals with the goal of developing gain media with broadband emission properties above 2 μm.

Single-crystals of CaF_2 codoped with 3-5 at.% Tm^{3+} and 0.3-0.5 at.% Ho^{3+} (with respect to Ca^{2+}) were grown by the Bridgman–Stockbarger technique using graphite crucibles (Φ8 mm, height: 40 mm). The starting reagents were CaF_2, TmF_3 and HoF_3 powders (purity: 4N), the rare-earth fluorides were achieved by fluorination of the corresponding oxides. A special attention was paid to reduce the oxygen contamination: the growth chamber was sealed to vacuum (<10^{-5} mbar) and refilled with Ar + CF_4 gases. The starting reagents were mixed and placed into the crucible which was heated slightly above (~40 °C) the melting point (1418 °C) and the solution was homogenized for 3-4 h. The growth was ensured by translating the crucible in a vertical temperature gradient of 30-40 °C/cm. After the growth was completed, the crystals were slowly cooled down to room temperature within 48 h. The segregation coefficients for Tm^{3+} and Ho^{3+} ions in CaF_2 are 0.94 and 0.98, respectively. The actual ion densities are N_{Tm} = 6.91 and N_{Ho} = 0.72 [10^{20} at/cm^3] for the 3 at.% Tm^{3+}, 0.3 at.% Ho^{3+}:CaF_2 crystal.

The as-grown crystals were transparent with a slight rose coloration due to Ho^{3+} doping, Fig. 1(a). A Schlieren photography of a polished cylindrical barrel cut from the central part of the crystal confirmed its high optical quality, Fig. 1(b).

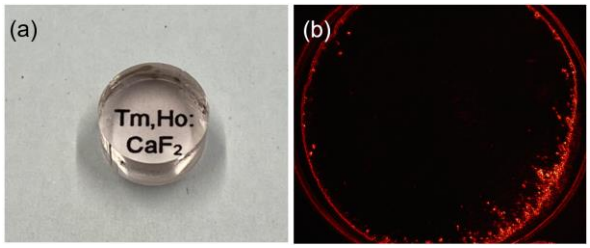

Fig. 1. (a) A photograph and (b) a Schlieren photography of a polished cylindrical barrel cut from the central part of an as-grown 3 at.% Tm^{3+}, 0.3 at.% Ho^{3+}:CaF_2 crystal.

The absorption spectra of Tm,Ho:CaF_2 crystals corresponding to the $^3H_6 \rightarrow {}^3H_4$ Tm^{3+} pump transition are shown in Fig. 2(a). The peak absorption cross-section σ_{abs} is 0.46×10^{-20} cm^2 at 768.1 nm and the corresponding bandwidth (full width at half maximum, FWHM) is 12.6 nm, which is beneficial for diode-pumping. Figure 2(b) shows the luminescence spectrum of a codoped crystal around 2 μm. It is smooth and broad spanning from 1.55 to 2.25 μm due to two spectrally overlapping transitions, $^3F_4 \rightarrow {}^3H_6$ Tm^{3+} and $^5I_7 \rightarrow {}^5I_8$ Ho^{3+}, with the Ho^{3+} emission peaking at 2025 nm being more intense. As compared to singly Ho^{3+}-doped crystals, the Tm^{3+},Ho^{3+} codoping induces additional broadening of the Ho^{3+} emission band due to more profound ion clustering at higher total RE^{3+} doping levels.

The absorption, σ_{abs}, and stimulated-emission cross-section, σ_{SE}, spectra for the $^5I_8 \leftrightarrow {}^5I_7$ Ho^{3+} transition in the 5 at.% Tm^{3+}, 0.5 at.% Ho^{3+} codoped CaF_2 crystal are shown in Fig. 2(c). The maximum σ_{SE} is 0.72×10^{-20} cm^2 at 2042 nm, as calculated using the Füchtbauer–Ladenburg formula. The $^5I_7$ radiative lifetime, τ_{rad} = 12.6 ms, was determined using a modified Judd-Ofelt theory [26]. According to the quasi-three-level nature of the Ho^{3+} laser scheme, the gain cross-sections for Ho^{3+} ions, $\sigma_{gain} = \beta\sigma_{SE} - (1-\beta)\sigma_{abs}$, were calculated for different inversion ratios $\beta = N_2/N_{Ho}$, where N_2 is the population of the upper laser level ($^5I_7$), Fig. 2(d). The gain profiles are smooth and broad and their maximum experiences a blue-shift with increasing the inversion ratio, from 2130 nm (β = 0.12) to 2040 nm (β = 0.30). For an intermediate β = 0.24, the gain bandwidth (FWHM) is 77 nm.

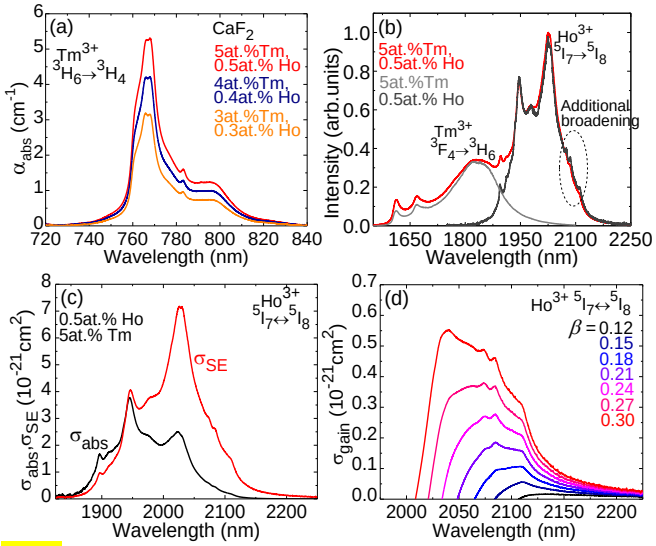

Fig. 2. Spectroscopy of Tm,Ho:CaF_2 crystals: (a) absorption spectra, the $^3H_6 \rightarrow {}^3H_4$ Tm^{3+} transition; (b) luminescence spectrum around 2 μm, 5 at.% Tm^{3+}, 0.5 at.% Ho^{3+} codoped crystal, the spectra for singly-doped crystals are given for comparison; (c,d) 5 at.% Tm^{3+}, 0.5 at.% Ho^{3+}:CaF_2 crystal, the $^5I_8 \leftrightarrow {}^5I_7$ Ho^{3+} transition: (c) absorption, σ_{abs}, and stimulated-emission, σ_{SE}, cross-sections, (d) gain cross-sections for Ho^{3+} ions, σ_{gain}, $\beta = N_2(^5I_7)/N_{Ho}$ – inversion ratio.

The luminescence decay curves from the $^3F_4$ Tm^{3+} and $^5I_7$ Ho^{3+} states were measured under resonant excitation for singly-doped 4 at.% Tm:CaF_2 and 0.5 at.% Ho:CaF_2 crystals, Fig. 3(a). The decay curves for both crystals are nearly single exponential yielding luminescence lifetimes τ_{lum} of 13.75 ms and 14.07 ms, respectively. The luminescence dynamics were studied for a 4 at.% Tm, 0.4 at.% Ho:CaF_2 crystal under resonant Tm^{3+} excitation, see Fig. 3(b). The decay curves are typical for the Tm^{3+},Ho^{3+} coupled systems indicating an efficient and predominantly unidirectional $^3F_4(Tm^{3+}) \rightarrow {}^5I_7(Ho^{3+})$ ET. The observation of two different time scales for the rise of Ho^{3+} luminescence and the beginning of the Tm^{3+} decay indicates the presence of two ion cluster compositions: (i) those containing both dopants and (ii) those being composed of only Tm^{3+} ions. The thermal equilibrium decay time for both ions is 11.0 ms.

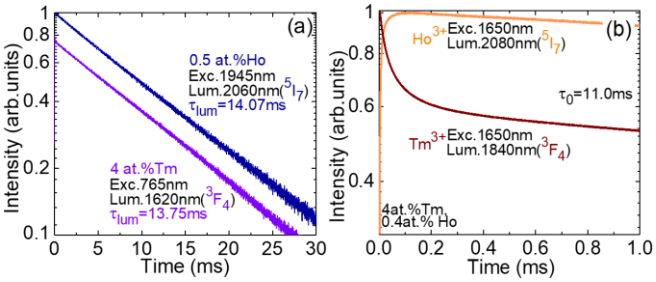

Fig. 3. Luminescence decay from the $^3F_4$ Tm^{3+} and $^5I_7$ Ho^{3+} states in CaF_2: (a) singly-doped crystals (4 at.% Tm^{3+} and 0.5 at.% Ho^{3+}), (b) a codoped crystal (4 at.% Tm^{3+}, 0.4 at.% Ho^{3+}).

A low-temperature (LT, 12 K) absorption spectrum of a 0.5 at.% Ho:CaF_2 crystal at ~2 μm is shown in Fig. 4(a). It shows sharp peaks assigned to isolated Ho^{3+} ions in trigonal (C_{3v}), tetragonal (C_{4v}) and cubic (O_h) sites, as well as intense and broader bands owing to Ho ion clusters. For a codoped crystal (5 at.% Tm^{3+}, 0.5 at.% Ho^{3+}), the LT absorption and emission spectra of Ho^{3+} ions for the $^5I_8 \leftrightarrow {}^5I_7$ transition, Fig. 4(a,b), contain just broad bands which are different from those for single Ho^{3+} doping indicating the entering of Ho^{3+} ions into rare-earth (Tm-Ho) ion clusters.

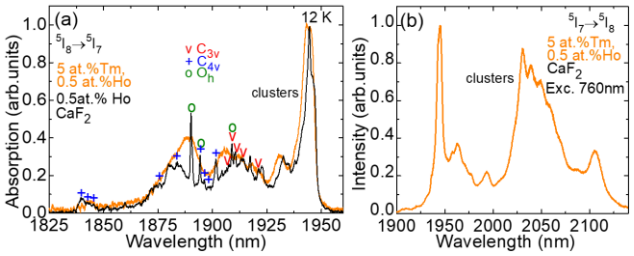

Fig. 4. LT (12 K) (a) absorption and (b) luminescence spectra of Ho^{3+} ions in CaF_2 ($^5I_8 \leftrightarrow {}^5I_7$ transition): a 5 at.% Tm^{3+}, 0.5 at.% Ho^{3+} codoped crystal and a 0.5 at.% Ho^{3+} singly-doped one.

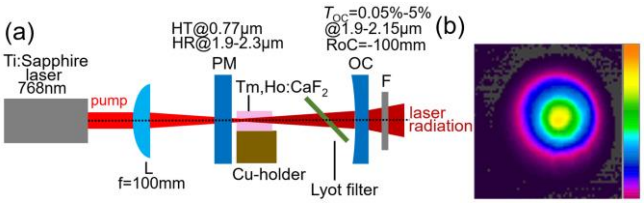

Fig. 5. (a) Set-up of the tunable Tm,Ho:CaF_2 laser: L- aspherical focusing lens, PM – pump mirror, OC – output coupler, F – long-pass filter; (b) a typical laser mode profile measured at 15 cm from the OC.

The scheme of the laser is depicted in Fig. 5(a). Cylindric laser elements (Φ8 mm, thickness: 4.1 mm) were cut from the central parts of the as-grown Tm,Ho:CaF_2 crystal boules with three doping levels, 5/0.5, 4/0.4 and 3/0.3 at.% Tm^{3+}/Ho^{3+}. They were polished to laser-quality on both sides and left uncoated. The elements were mounted on a Cu-holder using a silver paste for better heat removal. The crystals were passively cooled to benefit from the good thermal properties of CaF_2. The hemispherical laser cavity was formed by a flat pump mirror (PM) coated for high transmission (HT, T = 93%) at 0.77 μm and high reflection (HR) at 1.9 – 2.3 μm, and a set of concave output couplers (OCs) with a radius of curvature (RoC) of -100 mm and a transmission at the laser wavelength T_{OC} in the range of 0.05% - 5%. The cavity length was ~99 mm. The laser crystal was placed near the PM with a separation <1 mm. The pump source was a CW Ti:Sapphire laser (3900S, Spectra Physics) emitting up to 4.0 W at 768.0 nm with a nearly diffraction limited beam ($M^2 \approx 1$). The pump radiation was focused into the crystal through the PM using an antireflection (AR) coated aspherical lens (focal length, f = 100 mm). The pump spot size in the focus was $2w_P$ = 70±10 μm. The pumping was in double pass owing to a high reflectivity of the OCs at the pump wavelength. E.g., for the 3 at.% Tm^{3+}, 0.3 at.% Ho^{3+} codoped crystal, the total pump absorption under lasing conditions was ~76% being weakly dependent on the output coupling. Optionally, the pump beam was modulated using a mechanical chopper (duty cycle: 1:4). A long-pass filter (FEL1000, Thorlabs) was placed after the OC to filter out the residual pump. The laser spectra were recorded using an optical spectrum analyzer (AQ6376, Yokogawa) and a ZrF_4 fiber. The laser mode profile was captured using a Pyrocam IIIHR camera (Ophir-Spiricon).

The best laser performance was achieved for the 3 at.% Tm^{3+}, 0.3 at.% Ho^{3+}:CaF_2 crystal. In the CW regime, the Tm,Ho:CaF_2 laser generated a maximum output power of 737 mW at 2062-2088 nm with a slope efficiency η of 28.0% (vs. the absorbed pump power) and a low laser threshold P_{th} of 133 mW (for T_{OC} = 1%), as shown in Fig. 6(a). For higher output coupling (T_{OC} > 1%), the laser performance deteriorated which is attributed to the detrimental effect of ETU at increased populations of the upper laser level. For these OCs, a thermal roll-over was observed for P_{abs} > 2.2 W. With reducing the output coupling, the laser threshold gradually decreased from P_{th} = 312 mW (5% OC) to 65 mW (0.05% OC). Power scaling was limited by the available pump power.

The typical spectra of laser emission are shown in Fig. 3(b). The laser operated solely on the $^5I_7 \rightarrow {}^5I_8$ Ho^{3+} transition and no Tm^{3+} colasing was observed. The laser wavelength experienced a blue-shift with increasing T_{OC}, from 2090-2116 nm (0.05% OC) to 2032-2039 nm (5% OC). This behavior is due to the quasi-three-level nature of the Ho^{3+} laser scheme with reabsorption and it agrees well with the gain spectra of Ho^{3+} ions in CaF_2, see Fig. 2(d). The laser emission was unpolarized. The Tm,Ho:CaF_2 laser operated on the fundamental transverse mode, Fig. 5(b), with a measured beam quality factor M^2 < 1.1 at the highest output power.

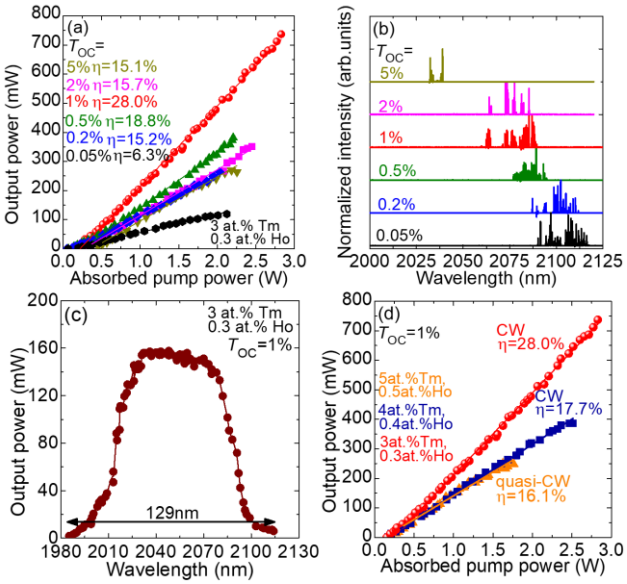

Fig. 6. CW Tm,Ho:CaF_2 lasers: (a-b) a 3 at.% Tm^{3+}, 0.3 at.% Ho^{3+} codoped crystal: (a) input-output dependences, η – slope efficiency; (b) typical laser emission spectra; (c) tuning curve, T_{OC} = 1%; (d) effect of the Tm^{3+} / Ho^{3+} doping level on the laser performance, T_{OC} = 1%.

For the wavelength tunable operation, a Lyot filter was inserted into the laser cavity at the Brewster angle close to the laser crystal. It was made of a 2 mm-thick quartz plate with an optical axis lying in the surface plane. When using T_{OC} = 1%, the laser wavelength was

continuously tunable from 1985 to 2114 nm (tuning range: 129 nm at the zero-power level).

The laser performance of Tm,Ho:CaF_2 crystals with different doping levels is compared in Fig. 6(d) (for the same T_{OC} = 1%). With increasing the doping level, despite the increased pump absorption, the maximum output power and the slope efficiency decreased to 386 mW at 2070-2086 nm with η = 17.7% (4 at.% Tm^{3+}, 0.4 at.% Ho^{3+}:CaF_2) and 249 mW at 2083-2087 nm with η = 16.1% (5 at.% Tm^{3+}, 0.5 at.% Ho^{3+}:CaF_2). For these crystals, a thermal roll-over in the output dependences was observed for absorbed pump powers above 2.5 W and 1.75 W, respectively (for the latter crystal, the laser was operated in quasi-CW regime). The observed deterioration of the laser performance is ascribed to a drop in the thermal conductivity of CaF_2 crystals upon rare-earth doping increase.

To conclude, we report on the first continuous-wave Tm,Ho:CaF_2 laser delivering an output power up to 737 mW at 2062-2088 nm with a maximum slope efficiency of 28.0% and a laser threshold down to 65 mW, operating on the fundamental transverse mode. A continuous wavelength tuning over a broad range of 129 nm (1985 - 2114 nm) was demonstrated. These results are superior to the previous reports on Tm,Ho:CaF_2 ceramic lasers (operating in free-running / quasi-CW regimes) [24,25], mainly due to the better optical and thermal properties of Tm,Ho:CaF_2 single-crystals. In the present work, the crystal quality was improved by carefully controlling the growth atmosphere. The spectroscopic properties of Ho^{3+} ions in Tm,Ho:CaF_2 crystals were also studied. They exhibit inhomogeneously broadened emission spectra extending above 2 µm (up to at least 2.25 µm) owing to the profound rare-earth ion clustering, an efficient $Tm^{3+} \rightarrow Ho^{3+}$ energy-transfer and a relatively long thermal equilibrium decay time. Evidence of existence of two cluster compositions (Tm and Tm/Ho clusters) is presented.

Thanks to its low melting point and good thermal properties, Tm,Ho:CaF_2 appears as an attractive competitor to other recently studied Tm^{3+},Ho^{3+}-codoped laser crystals with broadband emission properties, Tm,Ho:$CaGaAlO_4$ [15] and Tm,Ho:CNGG [28]. Further improvement of the laser efficiency for Tm,Ho:CaF_2 is possible by: optimizing the Ho^{3+}/Tm^{3+} codoping ratio to suppress the Ho-free Tm-clusters which do not contribute significantly to laser emission >2 µm, and implementing a Tm resonant pumping, e.g., by Raman-shifted Erbium fiber lasers [27]. Further power scaling is expected under pumping at ~0.8 µm using AlGaAs laser diodes and applying active cooling. In this case, lower total Tm+Ho doping levels are preferable for maintaining better thermal properties of Tm,Ho:CaF_2 crystals, as evidenced by the present work.

Funding. Agence Nationale de la Recherche (ANR-19-CE08-0028); Région Normandie (Chaire d'excellence "RELANCE").

Disclosures. The authors declare no conflicts of interest.

Data availability. Data underlying the results presented in this paper are not publicly available at this time but may be obtained from the authors upon reasonable request.

References

1. F. Druon, S. Ricaud, D. N. Papadopoulos, A. Pellegrina, P. Camy, J. L. Doualan, R. Moncorgé, A. Courjaud, E. Mottay, and P. Georges, Opt. Mater. Express **1**, 489 (2011).
2. P. Camy, J. L. Doualan, S. Renard, A. Braud, V. Ménard, and R. Moncorgé, Opt. Commun. **236**, 395 (2004).
3. C. Labbe, J. L. Doualan, P. Camy, R. Moncorgé, and M. Thuau, Opt. Commun. **209**, 193 (2002).
4. V. Petit, P. Camy, J.-L. Doualan, X. Portier, and R. Moncorgé, Phys. Rev. B **78**, 085131 (2008).
5. B. Lacroix, C. Genevois, J. L. Doualan, G. Brasse, A. Braud, P. Ruterana, P. Camy, E. Talbot, R. Moncorgé, and J. Margerie, Phys. Rev. B **90**, 125124 (2014).
6. P. Loiko, A. Braud, L. Guillemot, J.L. Doualan, A. Benayad, and P. Camy, Proc. SPIE **11357**, 113570N (2020).
7. G. Machinet, P. Sevillano, F. Guichard, R. Dubrasquet, P. Camy, J. L. Doualan, R. Moncorgé, P. Georges, F. Druon, D. Descamps, and E. Cormier, Opt. Lett. **38**, 4008 (2013).
8. C. Meroni, A. Braud, J. L. Doualan, C. Maunier, S. Montant, and P. Camy, J. Lumin. **252**, 119336 (2022).
9. K. Veselský, J. Šulc, H. Jelínková, M. E. Doroshenko, V. A. Konyushkin, and A. N. Nakladov, Laser Phys. Lett. **17**, 025802 (2020).
10. R. Thouroude, A. Tyazhev, A. Hideur, P. Loiko, P. Camy, J. L. Doualan, H. Gilles, and M. Laroche, Opt. Lett. **45**, 4511 (2020).
11. T. Y. Fan, G. Huber, R. L. Byer, and P. Mitzscherlich, IEEE J. Quantum Electron. **24**, 924 (1988).
12. P. Loiko, J. M. Serres, X. Mateos, K. Yumashev, N. Kuleshov, V. Petrov, U. Griebner, M. Aguiló, and F. Díaz, Opt. Express **22**, 27976 (2014).
13. S. Lamrini, P. Koopmann, M. Schäfer, K. Scholle, and P. Fuhrberg, Appl. Phys. B **106**, 315 (2012).
14. J. W. Kim, J. I. Mackenzie, D. Parisi, S. Veronesi, M. Tonelli, and W. A. Clarkson, Opt. Lett. **35**, 420 (2010).
15. Y. Wang, P. Loiko, Y. Zhao, Z. Pan, W. Chen, M. Mero, X. Xu, J. Xu, X. Mateos, A. Major, M. Guina, V. Petrov, and U. Griebner, Opt. Express **30**, 7883 (2022).
16. Y. Zhao, Y. Wang, X. Zhang, X. Mateos, Z. Pan, P. Loiko, W. Zhou, X. Xu, J. Xu, D. Shen, and S. Suomalainen, Opt. Lett. **43**, 915 (2018).
17. P. Forster, C. Romano, J. Schneider, M. Eichhorn and C. Kieleck, Opt. Lett. **47**, 2542 (2022).
18. R. Lan, P. Loiko, X. Mateos, Y. Wang, J. Li, Y. Pan, S. Y. Choi, M. H. Kim, F. Rotermund, A. Yasukevich, K. Yumashev, U. Griebner, and V. Petrov, Appl. Opt. **55**, 4877 (2016).
19. M. B. Seelbinder, and J. C. Wright, Phys. Rev. B **20**, 4308 (1979).
20. Yu. K. Voronko, A. A. Kaminskii, V. V. Osiko and A. M. Prokhorov, JETP Lett. **1**, 3 (1965).
21. M. Jelinek, V. Kubeček, W. Ma, B. Zhao, D. Jiang, and L. Su, Laser Phys. Lett. **13**, 065004 (2016).
22. M. Němec, J. Šulc, M. Jelínek, V. Kubeček, H. Jelínková, M. E. Doroshenko, O. K. Alimov, V. A. Konyushkin, A. N. Nakladov, and V. V. Osiko, Opt. Lett. **42**, 1852 (2017).
23. X. Duan, L. Li, X. Guo, Y. Ding, B. Yao, L. Zheng, L. Su, and Y. Wang, Opt. Express **26**, 26916 (2018).
24. J. Šulc, M. Němec, H. Jelinková, M. E. Doroshenko, P. P. Fedorov, and V. V. Osiko, Proc. SPIE **8959**, 895925 (2014).
25. J. Šulc, M. Němec, H. Jelínková, M. E. Doroshenko, P. P. Fedorov, and V. V. Osiko, in *Advanced Solid-State Lasers Congress* (Optica Publishing Group, 2013), paper AM4A.26.
26. P. Loiko, A. Volokitina, X. Mateos, E. Dunina, A. Kornienko, E. Vilejshikova, M. Aguilo, and F. Diaz, Opt. Mater. **78**, 495-501 (2018).
27. P. Loiko, E. Kifle, G. Brasse, R. Thouroude, F. Starecki, A. Benayad, A. Braud, M. Laroche, S. Girard, H. Gilles, and P. Camy, Opt. Express **30**, 11840 (2022).
28. Z. Pan, P. Loiko, Y. Wang, Y. Zhao, H. Yuan, X. Dai, H. Cai, J. M. Serres, S. Slimi, E. Dunina, A. Kornienko, J.-L. Doualan, P. Camy, U. Griebner, V. Petrov, M. Aguiló, F. Díaz, and X. Mateos, J. Alloys Compd. **853**, 157100-1-15 (2021).

Full references

1. F. Druon, S. Ricaud, D. N. Papadopoulos, A. Pellegrina, P. Camy, J. L. Doualan, R. Moncorgé, A. Courjaud, E. Mottay, and P. Georges, "On Yb:CaF_2 and Yb:SrF_2: review of spectroscopic and thermal properties and their impact on femtosecond and high power laser performance," Opt. Mater. Express **1**(3), 489-502 (2011).
2. P. Camy, J. L. Doualan, S. Renard, A. Braud, V. Ménard, and R. Moncorgé, "Tm^{3+}: CaF_2 for 1.9 µm laser operation," Opt. Commun. **236**(4-6), 395-402 (2004).
3. C. Labbe, J. L. Doualan, P. Camy, R. Moncorgé, and M. Thuau, "The 2.8 µm laser properties of Er^{3+} doped CaF_2 crystals," Opt. Commun. **209**(1-3), 193-199 (2002).
4. V. Petit, P. Camy, J.-L. Doualan, X. Portier, and R. Moncorgé, "Spectroscopy of Yb^{3+}:CaF_2: from isolated centers to clusters," Phys. Rev. B **78**(8), 085131-1-12 (2008).
5. B. Lacroix, C. Genevois, J. L. Doualan, G. Brasse, A. Braud, P. Ruterana, P. Camy, E. Talbot, R. Moncorgé, and J. Margerie, "Direct imaging of rare-earth ion clusters in Yb:CaF_2," Phys. Rev. B **90**(12), 125124-1-14 (2014).
6. P. Loiko, A. Braud, L. Guillemot, J.L. Doualan, A. Benayad, and P. Camy, "Cross-relaxation and ion clustering in Tm^{3+}:CaF_2 crystals," Proc. SPIE **11357**, 113570N (2020).
7. G. Machinet, P. Sevillano, F. Guichard, R. Dubrasquet, P. Camy, J. L. Doualan, R. Moncorgé, P. Georges, F. Druon, D. Descamps, and E. Cormier, "High-brightness fiber laser-pumped 68 fs-2.3 W Kerr-lens mode-locked Yb:CaF_2 oscillator," Opt. Lett. **38**(9), 4008-4010 (2013).
8. C. Meroni, A. Braud, J. L. Doualan, C. Maunier, S. Montant, and P. Camy, "Spectroscopy and laser gain measurements of CaF_2: Nd, X^{3+}, Z^{3+} (X, Z= Gd, La, Ce, Y, Lu, Sc) crystals for broadband lasers applications," J. Lumin. **252**, 119336 (2022).
9. K. Veselský, J. Šulc, H. Jelínková, M. E. Doroshenko, V. A. Konyushkin, and A. N. Nakladov, "Spectroscopic and laser properties of a broadly tunable diode-pumped Tm^{3+}: CaF_2–SrF_2 laser." Laser Phys. Lett. **17**(2), 025802-1-5 (2020).
10. R. Thouroude, A. Tyazhev, A. Hideur, P. Loiko, P. Camy, J. L. Doualan, H. Gilles, and M. Laroche, "Widely tunable in-band-pumped Tm:CaF_2 laser," Opt. Lett. **45**(16), 4511-4514 (2020).
11. T. Y. Fan, G. Huber, R. L. Byer and P. Mitzscherlich, "Spectroscopy, and diode laser-pumped operation of Tm,Ho:YAG," IEEE J. Quantum Electron. **24**(6), 924-933 (1988).
12. P. Loiko, J. M. Serres, X. Mateos, K. Yumashev, N. Kuleshov, V. Petrov, U. Griebner, M. Aguiló, and F. Díaz, "Microchip laser operation of Tm,Ho:$KLu(WO_4)_2$ crystal," Opt. Express **22**(23), 27976-27984 (2014).
13. S. Lamrini, P. Koopmann, M. Schäfer, K. Scholle, and P. Fuhrberg, "Efficient high-power Ho: YAG laser directly in-band pumped by a GaSb-based laser diode stack at 1.9 µm," Appl. Phys. B **106**(2), 315-319 (2012).
14. J. W. Kim, J. I. Mackenzie, D. Parisi, S. Veronesi, M. Tonelli, and W. A. Clarkson, "Efficient in-band pumped Ho:$LuLiF_4$ 2 µm laser," Opt. Lett. **35**(3), 420-422 (2010).
15. Y. Wang, P. Loiko, Y. Zhao, Z. Pan, W. Chen, M. Mero, X. Xu, J. Xu, X. Mateos, A. Major, M. Guina, V. Petrov, and U. Griebner, "Polarized spectroscopy and SESAM mode-locking of Tm,Ho:CALGO," Opt. Express **30**(5), 7883-7893 (2022).
16. Y. Zhao, Y. Wang, X. Zhang, X. Mateos, Z. Pan, P. Loiko, W. Zhou, X. Xu, J. Xu, D. Shen, and S. Suomalainen, "87 fs mode-locked Tm,Ho:$CaYAlO_4$ laser at ~2043 nm," Opt. Lett. **43**(4), 915-918 (2018).
17. P. Forster, C. Romano, J. Schneider, M. Eichhorn, and C. Kieleck, "High-power continuous-wave Tm^{3+}:Ho^{3+}-codoped fiber laser operation from 2.1 µm to 2.2 µm," Opt. Lett. **47**(17), 2542-2545 (2022).
18. R. Lan, P. Loiko, X. Mateos, Y. Wang, J. Li, Y. Pan, S. Y. Choi, M. H. Kim, F. Rotermund, A. Yasukevich, K. Yumashev, U. Griebner, and V. Petrov, "Passive Q-switching of microchip lasers based on Ho:YAG ceramics," Appl. Opt. **55**(18), 4877-4887 (2016).
19. M. B. Seelbinder, and J. C. Wright, "Site-selective spectroscopy of CaF_2: Ho^{3+}," Phys. Rev. B **20**(10), 4308-4320 (1979).
20. Yu. K. Voronko, A. A. Kaminskii, V. V. Osiko, and A. M. Prokhorov, "Stimulated emission of Ho^{3+} in CaF_2 at λ = 5512 Å," JETP Lett. **1**(1), 3-5 (1965).
21. M. Jelinek, V. Kubeček, W. Ma, B. Zhao, D. Jiang, and L. Su, "Cryogenic Ho:CaF_2 laser pumped by Tm:fiber laser," Laser Phys. Lett. **13**(6), 065004-1-5 (2016).
22. M. Němec, J. Šulc, M. Jelínek, V. Kubeček, H. Jelínková, M. E. Doroshenko, O. K. Alimov, V. A. Konyushkin, A. N. Nakladov and V. V. Osiko, "Thulium fiber pumped tunable Ho:CaF_2 laser," Opt. Lett. **42**(9), 1852-1855 (2017).
23. X. Duan, L. Li, X. Guo, Y. Ding, B. Yao, L. Zheng, L. Su, and Y. Wang, "Wavelength-locked continuous-wave and Q-switched Ho:CaF_2 laser at 2100.5 nm," Opt. Express **26**(21), 26916-26924 (2018).
24. J. Šulc, M. Němec, H. Jelinková, M. E. Doroshenko, P. P. Fedorov, and V. V. Osiko, "Diode pumped tunable lasers based on Tm:CaF_2 and Tm:Ho:CaF_2 ceramics," Proc. SPIE **8959**, 895925 (2014).
25. J. Šulc, M. Němec, H. Jelínková, M. E. Doroshenko, P. P. Fedorov, and V. V. Osiko, "Resonantly diode pumping of Tm:CaF_2 and Tm:Ho:CaF_2 lasers," in *Advanced Solid-State Lasers Congress*, G. Huber and P. Moulton, eds., OSA Technical Digest (online) (Optica Publishing Group, 2013), paper AM4A.26.
26. P. Loiko, A. Volokitina, X. Mateos, E. Dunina, A. Kornienko, E. Vilejshikova, M. Aguilo, and F. Diaz, "Spectroscopy of Tb^{3+} ions in monoclinic $KLu(WO_4)_2$ crystal application of an intermediate configuration interaction theory," Opt. Mater. **78**, 495-501 (2018).
27. P. Loiko, E. Kifle, G. Brasse, R. Thouroude, F. Starecki, A. Benayad, A. Braud, M. Laroche, S. Girard, H. Gilles, and P. Camy, "In-band pumped Tm,Ho:$LiYF_4$ waveguide laser," Opt. Express **30**(7), 11840-11847 (2022).
28. Z. Pan, P. Loiko, Y. Wang, Y. Zhao, H. Yuan, X. Dai, H. Cai, J. M. Serres, S. Slimi, E. Dunina, A. Kornienko, J.-L. Doualan, P. Camy, U. Griebner, V. Petrov, M. Aguiló, F. Díaz, and X. Mateos, "Disordered Tm^{3+},Ho^{3+}-codoped CNGG garnet crystal: Towards efficient laser materials for ultrashort pulse generation at ~2 µm," J. Alloys Compd. **853**, 157100-1-15 (2021).